

Spin-orbit coupling manipulating composite topological spin textures in atomic-molecular Bose-Einstein condensates

Chao-Fei Liu,^{1,2} Gediminas Juzeliūnas,³ and W. M. Liu²

¹*School of Science, Jiangxi University of Science and Technology, Ganzhou 341000, China*

²*Beijing National Laboratory for Condensed Matter Physics, Institute of Physics, Chinese Academy of Sciences, Beijing 100190, China*

³*Institute of Theoretical Physics and Astronomy, Vilnius University, A. Goštauto 12, 01108 Vilnius, Lithuania*

(Received 16 June 2016; published 24 February 2017)

Atomic-molecular Bose-Einstein condensates (BECs) offer brand new opportunities to revolutionize quantum gases and probe the variation of fundamental constants with unprecedented sensitivity. The recent realization of spin-orbit coupling (SOC) in BECs provides a new platform for exploring completely new phenomena unrealizable elsewhere. In this study, we find a way of creating a Rashba-Dresselhaus SOC in atomic-molecular BECs by combining the spin-dependent photoassociation and Raman coupling, which can control the formation and distribution of a different type of topological excitation—carbon-dioxide-like skyrmion. This skyrmion is formed by two half-skyrmions of molecular BECs coupling with one skyrmion of atomic BECs, where the two half-skyrmions locate at both sides of one skyrmion. Carbon-dioxide-like skyrmion can be detected by measuring the vortices structures using the time-of-flight absorption imaging technique in real experiments. Furthermore, we find that SOC can effectively change the occurrence of the Chern number in k space, which causes the creation of topological spin textures from some separated carbon-dioxide-like monomers each with topological charge -2 to a polymer chain of the skyrmions. This work helps in creating dual SOC atomic-molecular BECs and opens avenues to manipulate topological excitations.

DOI: [10.1103/PhysRevA.95.023624](https://doi.org/10.1103/PhysRevA.95.023624)

I. INTRODUCTION

Topological spin textures, such as skyrmion and half-skyrmion, have great advantages to be applied in future memory storage [1,2]. Containing the skyrmions' creation and annihilation processes, the formation of skyrmions' composite structures, which would lead to higher stability and more degrees of freedom for manipulating, is the intriguing and important issue to be addressed [2]. Single skyrmion and skyrmion lattices in spinor Bose-Einstein condensates (BECs) have been well understood in the past few years. But it is hard for skyrmions and half-skyrmions to form composite structures due to the superfluid property of BECs themselves.

The production of atomic-molecular BECs via the Raman photoassociation [3–9] has revolutionized the field of ultracold quantum gases because molecules offer microscopic degrees of freedom beyond atomic gases. In particular, spin-orbit coupling (SOC) in ultracold gases of atomic bosons [10–15] and fermions [16,17] provides a possible way to further design the topological excitations. This raises a question regarding how to create SOC in the mixed atomic-molecular BECs, which would be a dual platform for realizing SOC in both atoms and molecules at the same time. Undoubtedly, the SOC atomic-molecular BECs are a brand new system and may hold some special features that do not present in single atomic or molecular BECs.

The SOC, which describes the interaction of the particle's spin with its orbital motion, represents a fascinating and fast-developing area of research significantly overlapping with traditional condensed matter physics, but more importantly it could also contain completely new phenomena unrealizable elsewhere. Novel effects have been reported, such as formation of the Bose mixture exhibiting a phase-separated propagation [10], as well as appearance of the plane wave and stripe phases [18–20] and other nontrivial structures [21–33] in the SOC

atomic BECs. A number of schemes have been proposed to create general gauge fields and SOC for ultracold atoms [34–38]. Differing from the normal SOC ultracold atoms, the SOC atomic-molecular BECs would initiate the exploration of SOC to the untouched hybrid quantum systems.

In this study, we present a way of creating a dual equal-Rashba-Dresselhaus SOC in the atomic-molecular BECs by combining the spin-dependent photoassociation [39,40] and Raman coupling [10–15]. Since SOC is introduced in both atoms and molecules, we call it as dual SOC. Meanwhile, the rotating atomic-molecular BECs indeed support a new type of composite topological spin texture of topological charge -2 , which is named the carbon-dioxide-like skyrmion as it resembles a carbon-dioxide molecule, i.e., one skyrmion of atomic BECs locates between two half-skyrmions of molecular BECs, locking them as a pair. By examining the Chern number in k space, we find that this system has a large Chern number up to 10 or more. And SOC can promote the Chern number, which stands for the topological excitations, to be induced in the high- $|k|$ region, and suppress it in the low- $|k|$ region. Thus, we can use SOC to effectively change the configuration of topological spin textures. Our results not only indicate the immanent mechanism of a single carbon-dioxide-like skyrmion and the skyrmion chain according to the vortices configurations but also apply the Chern number to explain the reason for SOC inducing these topological excitations.

A. Creation of dual equal-Rashba-Dresselhaus spin-orbit coupling in atomic-molecular BECs

We consider a Bose gas of ultracold ^{87}Rb atoms, commonly used in both experiments on the SOC atomic BEC [10–15] and the atomic-molecular BECs [3,4], to demonstrate the scheme for creating SOC atomic-molecular BECs [see Fig. 1(a)]. We

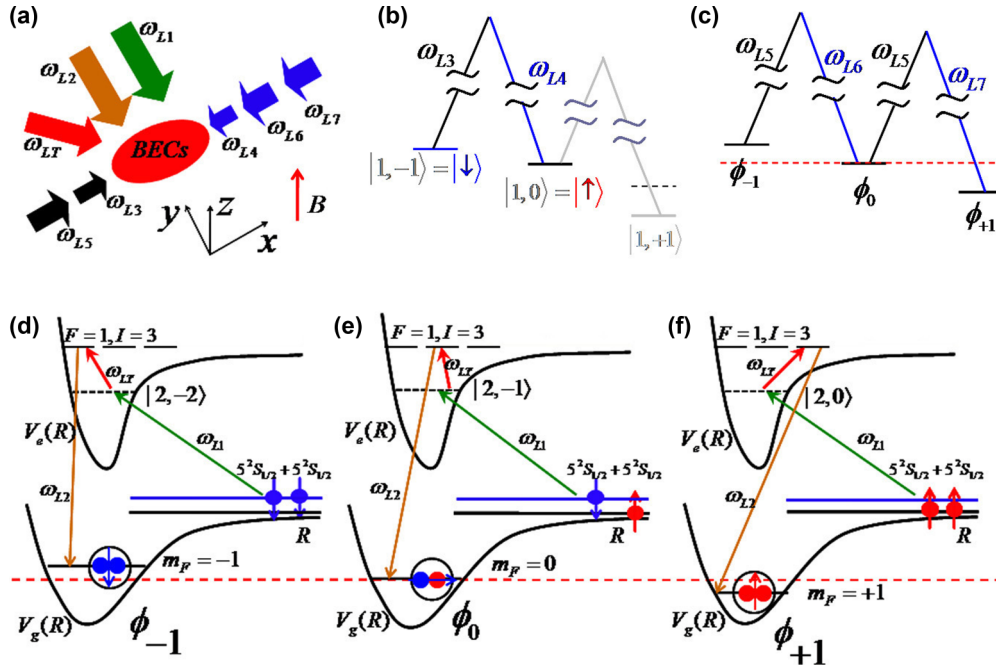


FIG. 1. Experimental setup for creating the spin-orbit coupled atomic-molecular BECs of ^{87}Rb . (a) The experimental geometry. The formation of spin molecular BECs: Laser field $L1$ finishes the spin-dependent photoassociation [39], laser field LT performs the $\Delta F = -1$, $\Delta m_F = +1$ is the transiting process of the excited molecules, and laser field $L2$ induces the excited molecules to emit a photon and forms the stable spin-1 molecular BECs. The creation of dual SOC: The laser fields $L3$ and $L4$ ($L5$, $L6$, and $L7$) are used to create the SOC of atomic (molecular) BECs along the x axis. B denotes a weak magnetic field along the z axis, which is used to induce the Zeeman shift. (b) Level diagram of Raman coupling within the atomic BECs. Two lasers ($L3$ and $L4$) are used to couple states of $|\uparrow\rangle$ (i.e., $|1, -1\rangle$) and $|\downarrow\rangle$ (i.e., $|1, 0\rangle$). (c) Level diagram of Raman coupling within the $F = 1$ molecular BECs. The three lasers ($L5$, $L6$, and $L7$) couple states of ϕ_{-1} , ϕ_0 , and ϕ_{+1} . (d) The procedure of creating $|F = 1, m_F = -1\rangle$ state molecular BEC. A close pair of atoms from the condensate in a state $|\downarrow\rangle$ absorb a photon from laser field $L1$ and then transit to a bound excited molecular state $|F = 2, m_F = -2\rangle$, i.e., the spin-dependent photoassociation process $|1, -1\rangle \otimes |1, -1\rangle \rightarrow |2, -2\rangle$ [39]. Via the laser field LT , the excited molecule transits to $|F = 1, m_F = -1\rangle$ state. Finally, laser field $L2$ induces the excited molecular state to emit a photon into molecular state ϕ_{-1} which keeps $F = 1$ and $m_F = -1$. Panels (e) and (f) are the procedure of creating $|F = 1, m_F = 0\rangle$ and $|F = 1, m_F = +1\rangle$ state molecular BECs, respectively.

take a BEC of up to 3×10^5 atoms and select two atomic internal spin states with $m_f = -1$ and $m_f = 0$ of the ^{87}Rb $5S_{1/2}$ ground state $f = 1$ manifold, to be described as the (pseudo-) spin up ($|\uparrow\rangle$) and down ($|\downarrow\rangle$) states [see Fig. 1(b)]. Here f and m_f are the quantum numbers of the atomic total spin and its projection along a quantization axis. A pair of counterpropagating Raman lasers (ω_{L3} and ω_{L4}) couple these spin states with the matrix element (Raman Rabi frequency) Ω_A inducing the SOC of the atomic BECs [see Fig. 1(b)]. The third spin state with $m_f = 1$ is detuned away from the Raman resonance due to the quadratic Zeeman shift and hence can be neglected. On the other hand, the counterpropagating Raman lasers (ω_{L5} , ω_{L6} , and ω_{L7}) are used to induce the SOC for the spin-1 ($F = 1$) molecular BECs [see Fig. 1(c)]. An extra laser ω_{L7} is needed to couple the molecular states with $m_F = 0$ and $m_F = 1$ detuned from the resonance between the states $m_F = -1$ and $m_F = 0$ due to a quadratic Zeeman effect. To prevent population of the excited state the laser fields are sufficiently detuned from the single photon resonance. The detailed processes for characterizing the dual SOC atomic-molecular BECs are indicated in the Appendix.

The molecular BECs of $^{87}\text{Rb}_2$ with hyperfine state $|F = 1, m_F = 0, \pm 1\rangle$ are produced by the spin-dependent photoassociation of atoms [39,40] [see Figs. 1(d)–1(f)]. A pair

of atoms with various combinations of internal states are coupled to an excited molecule state $|\phi_{em}\rangle$ via a laser beam ω_{L1} . Here the photoassociation through the total spin-2 scattering channel gives molecular F numbers of 2. The three spin-dependent photoassociation processes can be written as follows: $|1, 0\rangle \otimes |1, 0\rangle \rightarrow |2, 0\rangle$, $|1, -1\rangle \otimes |1, 0\rangle \rightarrow |2, -1\rangle$, and $|1, -1\rangle \otimes |1, -1\rangle \rightarrow |2, -2\rangle$. Under the transition $\Delta F = -1$ and $\Delta m_F = +1$, the excited molecule states further change into $|\phi'_{em}\rangle$ with $F = 1$ and $I = 3$ [39], where F , m_F , and I denote the total spin, its projection, and the nuclear spin quantum numbers of a molecule. Finally, $|\phi'_{em}\rangle$ is coupled to a ground molecule state $|\phi_m\rangle$ via another laser beam ω_{L2} [see Figs. 1(d)–1(f)]. As a result, the two-component atomic BEC can be coherently converted into a three-component (spin-1) molecular BEC with three internal spin states $|F = 1, m_F = 0, \pm 1\rangle$.

Our schematic has shown a possible method to create dual SOC atom-molecule BECs. In real experiments, the realization of dual SOC atom-molecule BECs would be affected by many factors, such as spontaneous Raman scattering by molecules, the inelastic collision channels between atoms and molecules, heating due to spontaneous scattering, some undesired light shifts, and inhomogeneous detuning of the laser fields [3–8]. For simplicity, we ignore the above factors. The dual SOC

atomic-molecular BECs can be described by (see Appendix):

$$\begin{aligned}
 i\hbar \frac{\partial \psi_a}{\partial t} &= \left[-\frac{\hbar^2 \nabla_d^2}{2M_A} + V_A + \sum_{q=\uparrow, \downarrow} g_{a,q} |\psi_q|^2 \right. \\
 &\quad \left. + \sum_{m=0, \pm 1} g_{a,m} |\phi_m|^2 \right] \psi_a + \lambda \sum_{q=\uparrow, \downarrow} (\hat{\sigma}_z)_{aq} p_x \psi_q \\
 &\quad + \hbar \Omega_A \sum_{q=\uparrow, \downarrow} (\hat{\sigma}_x)_{aq} \psi_q + K_a, \quad (1) \\
 i\hbar \frac{\partial \phi_m}{\partial t} &= \left[-\frac{\hbar^2 \nabla_d^2}{2M_M} + V_M + \sum_{q=\uparrow, \downarrow} g_{m,q} |\psi_q|^2 + g_n |\phi|^2 \right] \phi_m \\
 &\quad + 2\hbar \Omega_A \sum_{n=0, \pm 1} (\hat{F}_x)_{mn} \phi_n + \lambda \sum_{n=0, \pm 1} (\hat{F}_z)_{mn} p_x \phi_n \\
 &\quad + g_s \sum_{\alpha=x, y, z} \sum_{n, k, l=0, \pm 1} (\hat{F}_\alpha)_{mn} (\hat{F}_\alpha)_{kl} \phi_n \phi_k^* \phi_l + K_m, \quad (2)
 \end{aligned}$$

with $K_\uparrow = \sqrt{2}\chi\psi_\uparrow^*\phi_{+1} + \chi\psi_\downarrow^*\phi_0$, $K_\downarrow = \sqrt{2}\chi\psi_\downarrow^*\phi_{-1} + \chi\psi_\uparrow^*\phi_0$, $K_{+1} = \frac{\chi}{\sqrt{2}}\psi_\uparrow^2 + (\varepsilon + M_A\lambda^2)\phi_{+1}$, $K_0 = \chi\psi_\uparrow\psi_\downarrow + \varepsilon\phi_0$, and $K_{-1} = \frac{\chi}{\sqrt{2}}\psi_\downarrow^2 + (\varepsilon + M_A\lambda^2)\phi_{-1}$. Here $a = \uparrow, \downarrow$ and $m = 0, \pm 1$ label, respectively, the atomic and molecular spins; $d = 1, 2, 3$ refers to the dimension of the system; M_A (M_M) is the mass of the atom (molecule); $V_A = \frac{M_A\omega^2 r^2}{2}$ ($V_M = \frac{M_M\omega^2 r^2}{2}$) is the harmonic trap for atomic (molecular) BECs; $\hat{F}_{\alpha=x, y, z}$ ($\hat{\sigma}_{\alpha=x, y, z}$) are the spin-1 (Pauli) matrices; $g_{a,q} = \frac{4\pi\hbar^2 a_{aq}}{M_A}$ and $g_{a,m} = \frac{2\pi\hbar^2 a_{am}}{M_A M_M / (M_A + M_M)}$ are, respectively, the strengths of atom-atom and atom-molecule interaction; and g_n and g_s are the strengths of the spin-independent and spin-dependent interactions between the molecules. Here also ψ_a and ϕ_m denote the macroscopic wave functions of the atomic BEC in the internal state $|a\rangle$ ($a = \uparrow, \downarrow$) and those of the molecular BEC in the internal state $|m_F = m\rangle$ ($m = 0, \pm 1$). The parameters λ , Ω_A , χ , ε , and ω are the strengths of dual SOC, Raman coupling, atom-molecule conversion, Raman detuning, and trap frequency, respectively.

B. The numerical method for simulations

The damped projected Gross-Pitaevskii equation (PGPE) [41] is used to obtain the ground state of atomic-molecular BECs. By neglecting the noise term according to the corresponding stochastic PGPE [42], the damped PGPE for the atomic-molecular BECs is described as

$$d\psi_a = \mathcal{P} \left\{ -\frac{i}{\hbar} \hat{H}_a \psi_a dt + \frac{\gamma_a}{k_B T} (\mu_a - \hat{H}_a) \psi_a dt \right\}, \quad (3)$$

$$d\phi_m = \mathcal{P} \left\{ -\frac{i}{\hbar} \hat{H}_m \phi_m dt + \frac{\gamma_m}{k_B T} (\mu_m - \hat{H}_m) \phi_m dt \right\}, \quad (4)$$

where $\hat{H}_a \psi_a = i\hbar \frac{\partial \psi_a}{\partial t}$ ($a = \uparrow, \downarrow$), $\hat{H}_m \phi_m = i\hbar \frac{\partial \phi_m}{\partial t}$ ($m = 0, \pm 1$), T is the final temperature, k_B is the Boltzmann constant, and μ_a and μ_m are the chemical potential of atom and molecule respectively. γ_a (γ_m) is the growth rate for the a th component (m th component). To obtain the ground state, we set the parameter $\frac{\gamma_a}{k_B T} = \frac{\gamma_m}{k_B T} = 0.05$ directly. The projection operator

\mathcal{P} is used to restrict the dynamics of atomic-molecular BEC in the coherent region. The initial state of each component is generated by sampling the grand-canonical ensemble for a free ideal Bose gas with the chemical potential $\mu_{m,0} = 2\mu_{a,0}$. The final chemical potential of the noncondensate band is altered to the values $\mu_m = 2\mu_a$.

In this study, we mainly focus on the two-dimensional BECs. We use the parameters of atomic-molecular BECs of ^{87}Rb with $M_M = 2M_A$ ($M_A = 144.42 \times 10^{-27}$ Kg), the trapping frequency $\omega = 200 \times 2\pi$ Hz, and the strength of the atom-atom interaction $g_{\uparrow, \uparrow} = g_A$ with the scattering length $a_A = 101.8a_B$, where a_B is the Bohr radius. In addition, when the change in energy of converting two atoms into one molecule ($\Delta U = 2U_{Ta} - U_{Tm}$) [3], without including internal energy, approaches zero, we can obtain the value $2g_A = g_M$, and we set $g_n = g_M = 2g_A$. For simplicity, we set the atom-molecule interaction $g_{\uparrow, -1} = g_{\uparrow, 0} = g_{\uparrow, +1} = g_{\downarrow, -1} = g_{\downarrow, 0} = g_{\downarrow, +1} = g_{AM}$. The unit of length, time, and energy correspond to $\sqrt{\hbar/(M_A\omega)}$ ($\approx 0.76 \mu\text{m}$), ω^{-1} ($\approx 0.96 \times 10^{-3}$ s), and $\hbar\omega$, respectively. To excite vortices in this system, we add the rotation mechanism [23,43,44]. To obtain the rotating SOC BECs in real experiments, one method is to rotate the lasers creating SOC for an isotropic trap or to rotate both the lasers creating SOC and an anisotropic trap [43]. This leads to an effective time-independent Hamiltonian, $H_{\text{eff}} = H - \Omega_{\text{rotation}} L_z$, which describes the system in a rotating frame of reference [where $L_z = -i\hbar(x\partial_y - y\partial_x)$ is the orbital angular momentum operator and Ω_{rotation} is the frequency of rotation].

C. A single carbon-dioxide-like skyrmion in the dual SOC atomic-molecular BECs

Spin texture excitations, such as skyrmion and half-skyrmion, are particle-like topological entities in a continuous field and they play an important role in many condensed matter systems [1,2,45–47]. skyrmion has a nontrivial topological charge of absolute value 1 and half-skyrmion proposes the nontrivial topological charge of absolute value $\frac{1}{2}$. Usually, spin texture excitations relate to some vortices structure [48,49]. Specially, spin texture excitations would display variable configurations but the topological charge is fixed. The dual SOC atomic-molecular BECs provide a new platform for exploring the spin texture excitations coming from atomic BECs and molecular BECs simultaneously. Now we present a way to obtain a single carbon-dioxide-like skyrmion, which consists of one skyrmion with the topological charge -1 in the atomic BECs and two half-skyrmions with the topological charge $-\frac{1}{2}$ in the molecular BECs. On both sides of the skyrmion are the two half-skyrmions and they couple as a unity resembling the carbon dioxide molecule.

In Fig. 2, we set the initial chemical potential $\mu_{m,0} = 2\mu_{a,0} = 8\hbar\omega$ in the numerical simulations. The final chemical potential of the noncondensate band is increased to $\mu_m = 2\mu_a = 28\hbar\omega$. The densities and the corresponding phases of the dual SOC atomic-molecular BECs are obtained for the equilibrium state [see Figs. 2(a) and 2(b)]. One can see that both components of atomic BECs contain a vortex excitation. The spin-up (spin-down) component fills in the vortex of the spin-down (spin-up) component. Thus, this structure is similar to a vortices molecule [50]. At the same time, two vortices

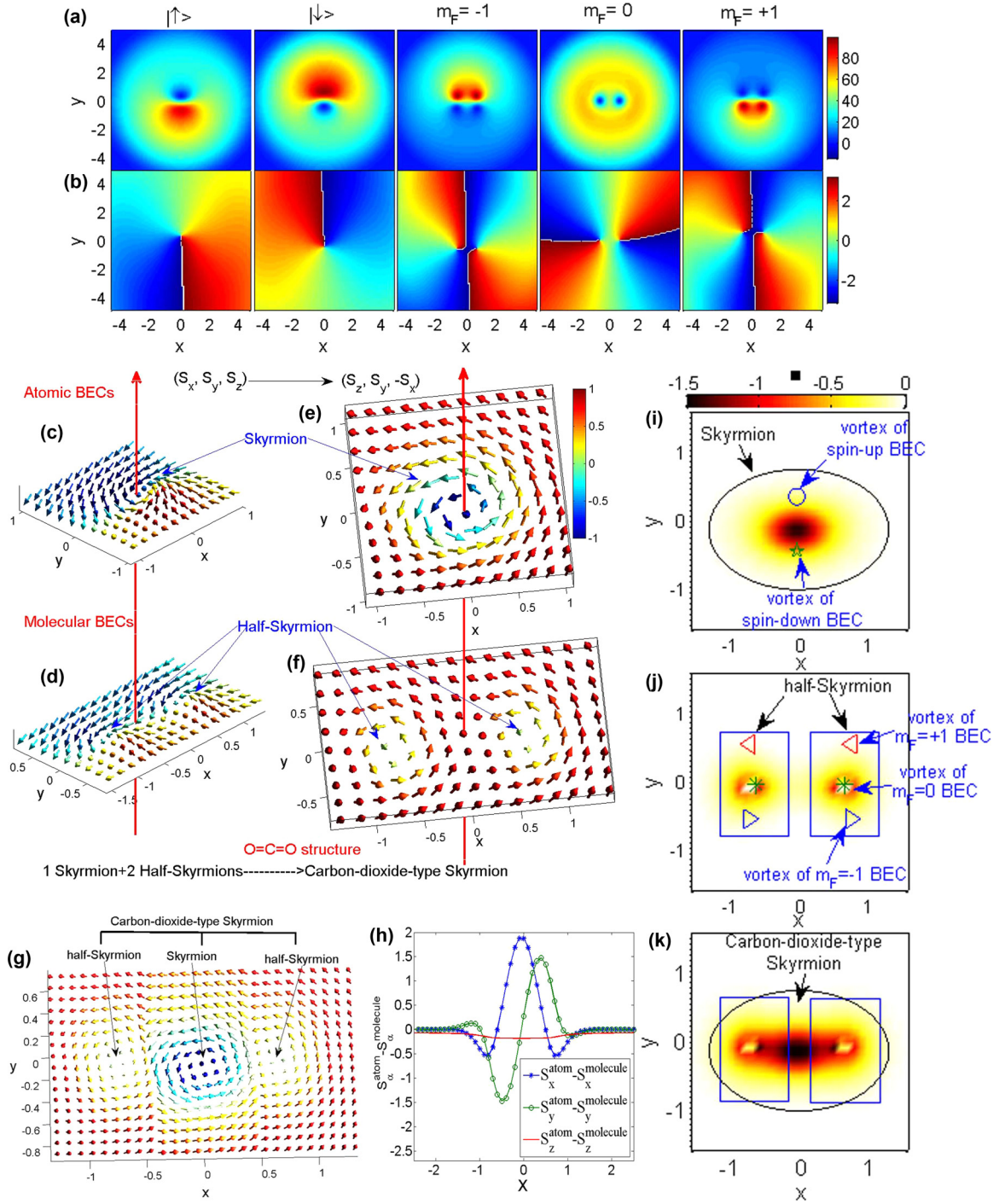


FIG. 2. Creating a carbon-dioxide-like skyrmion in the dual SOC atomic-molecular BECs. (a) The densities of each component when the system reaches the equilibrium state. The particles number $(N_{\uparrow}, N_{\downarrow}, N_{-1}, N_0, N_{+1})$ is $(2.56 \times 10^3, 2.98 \times 10^3, 1.72 \times 10^3, 3.22 \times 10^3, 1.59 \times 10^3)$. (b) The corresponding phases of each component in (a). [(c) and (d)] The spin texture of the atomic BECs and molecular BECs, respectively. The color of each arrow indicates the magnitude of S_z . [(e) and (f)] The corresponding spin texture under the transformation: $(S_x', S_y', S_z') = (S_z, S_y, -S_x)$. (g) A combined scheme of the carbon-dioxide-like skyrmion. A skyrmion (center) couples with two half-skyrmions, which have to be arranged at the two sides of the skyrmion. (h) The difference of spin vectors between the atomic BECs and the molecular BECs, where $y = 0$. [(i) and (j)] The topological charge density of the atomic BECs and molecular BECs, respectively. The ellipse and rectangles mark out the regions of a skyrmion and two half-skyrmions, respectively. The symbol \circ , \star , \triangleright , \ast , and \triangleleft are the position of vortices formed by the \uparrow , \downarrow , $m_F = -1$, $m_F = 0$, and $m_F = +1$ components, respectively. (k) The sum of the topological charge densities. It denotes the creation of carbon-dioxide-like skyrmion that the ellipse overlaps with the two rectangles. The unit of length, strength of χ , Ω_A and dual SOC are $0.76 \mu\text{m}$, $\hbar\omega$, ω , and $0.96 \times 10^{-3} \text{ m/s}$, respectively.

are induced in each molecular component, respectively. The densities of all the components are symmetric with respect to the y axis. In addition, only the density of the $m_F = 0$ component is symmetric with respect to the x axis. In this way, these vortices form a cluster.

The emergence of the vortices cluster results from a combination of the dual SOC, Raman coupling, atom-molecule conversion, and rotation effect. The dual equal-Rashba-Dresselhaus SOC causes a translational displacement along the y axis on the rotating BECs. The translational displacement for different spin state is opposite. Thus, the spin-up and $m_F = +1$ components tend to move to the $y < 0$ region, and the spin-down and $m_F = -1$ components go to the $y > 0$ region. Note that the $m_F = 0$ component is not affected by the SOC. Rotation induces vortices. In the atomic BECs, the spin-up and the spin-down component have to fill with each other in the region of the vortices. A similar case occurs in the molecular BECs with the vortices of the $m_F = 0$ component locating at the center. The atom-molecule conversion forces the atomic vortex of spin-up (spin-down) component to couple with two molecular ones of $m_F = +1$ ($m_F = -1$) components, just like that in the normal atomic-molecular BECs [51]. This leads to the formation of the above vortices cluster.

Since our system includes the pseudo-spin-1/2 atomic BECs and the spin-1 molecular BECs, there will be spin textures coming from atomic BECs and molecular BECs, respectively. Thus, this mixed system will show the interaction of the spin textures induced by different hyperfine spin states. In pseudo-spin-1/2 BECs and spin-1 BECs, the spin textures [50,52–54] are defined by $\mathbf{S}_\alpha^{\text{atom}} = \sum_{m,n=\uparrow\downarrow} \psi_m^* (\hat{\sigma}_\alpha)_{m,n} \psi_n / |\psi|^2$ and $\mathbf{S}_\alpha^{\text{molecule}} = \sum_{m,n=0,\pm 1} \phi_m^* (\hat{F}_\alpha)_{m,n} \phi_n / |\phi|^2$, ($\alpha = x, y, z$), where $\hat{\sigma}_\alpha$ and \hat{F}_α are the Pauli and spin-1 matrices, respectively. The spin textures in the atomic BECs and molecular BECs are shown in Figs. 2(c) and 2(d), respectively. In Fig. 2(c), the arrows form a circle locating near the position (0,0). The arrows tend to point down in the region $y < 0$ and to point up in the region $y > 0$. Similarly, in Fig. 2(d), the arrows form two half circles locating near the positions (0, -0.7) and (0, 0.7), respectively. Performing a transformation $(\mathbf{S}'_x, \mathbf{S}'_y, \mathbf{S}'_z) = (\mathbf{S}_z, \mathbf{S}_y, -\mathbf{S}_x)$, one can identify clearly a skyrmion [see Fig. 2(e)] and two half-skyrmions [see Fig. 2(f)]. In the Supplemental Material [55], we have proved that the transformation does not affect the value of the topological charge Q [$Q = \frac{1}{4\pi} \int \int q(x,y) dx dy$, where $q(x,y) = \mathbf{s} \cdot (\frac{\partial \mathbf{s}}{\partial x} \times \frac{\partial \mathbf{s}}{\partial y})$, $\mathbf{s} = \mathbf{S}/|\mathbf{S}|$]. Additionally, we provide approximate solutions for the carbon-dioxide-like skyrmion (see the Supplemental Material [55]). Figure 2(g) is a combined schematic of a carbon-dioxide-like skyrmion, where a skyrmion of atomic BECs couples with two half-skyrmions of molecular BECs. Figure 2(h) shows the differences of spin vectors between the atomic BECs and the molecular BECs ($y = 0$). It indicates that the spin vectors of atomic BECs and molecular BECs would tend to be parallel to each other, except those at the region of the carbon-dioxide-like skyrmion. Figures 2(i) and 2(j) show the topological charge density $q(x,y)$. The positions of vortices are pointed out to highlight the relationship between skyrmion and vortices. We find that the topological charge approaches -1 and $-\frac{1}{2}$ for the two types of spin texture, respectively. The two zero points in

the Fig. 2(j) further prove that we obtain two half-skyrmions. Figure 2(k) shows the sum of topological charge density [i.e., $q_{\text{sum}}(x,y) = q_{\text{atom}}(x,y) + q_{\text{molecule}}(x,y)$], which further clearly indicates the carbon-dioxide-like structure.

D. The chain of carbon-dioxide-like skyrmion in the dual SOC atomic-molecular BECs.

To fully show why SOC changes the spin textures, we now further demonstrate the effect of the dual SOC on the rotating atomic-molecular BECs in Fig. 3. We change the initial chemical potential and final chemical potential to be $\mu_m = 2\mu_a = 3.5\mu_{m,0} = 7\mu_{a,0} = 42\hbar\omega$. Figures 3(a), 3(c), and 3(e) display densities of the atomic-molecular BECs obtained for the equilibrium state at $\Omega_{\text{rotation}} = 0.5\omega$. Figures 3(b), 3(d), and 3(f) demonstrate the corresponding phases. Without the dual SOC ($\lambda = 0$), two atomic and three molecular components of the BECs do not display the phase separation [see Fig. 3(a)]. Yet there are a lot of vortices in each component, and they can be identified by the phase image [see Fig. 3(b)]. However, adding the dual SOC ($\lambda = 1$), the two components of atomic BECs separate [see Fig. 3(c)]. The component described by ψ_\uparrow mainly locates below the x axis, whereas ψ_\downarrow mainly locates above the x axis. Similarly, the phase separation also occurs in the molecular BECs. Because the spin-up (spin-down) atoms can form the ϕ_{+1} (ϕ_{-1}) component, the corresponding molecular BECs of ϕ_{+1} (ϕ_{-1}) also tends to locate below (above) $y = 0$ axis. The ϕ_0 component is spread around the x direction and squeezed in the y direction, and the area is filled with vortices. When the strength of the dual SOC is up to $\lambda = 2$, the phase separation becomes more obvious [see Fig. 3(e)]. In fact, the phase separation does not take place at all if the rotation is absent. Therefore, the combination of dual SOC and rotation induces the phase separation in the atomic-molecular BECs.

To detect the underlying relationship between the topological excitations, Figures 3(g)–3(i) show the position of vortices, where the results correspond to Figs. 3(a), 3(c), and 3(e), respectively. Note that we do not indicate the vortices where the densities of BECs are very low. In that case, the contribution of energy and momentum to the system almost can be neglected. Without the dual SOC [see Fig. 3(g)] five types of vortices form certain clusters (a black rectangle shows an example). The repulsion among vortices of each component forces them to spread around the whole BECs, but they do not form a regular lattice. At the same time, the repulsion among vortex clusters also leads to the deformation of the clusters shown in Fig. 3(g). In Fig. 3(h) ($\lambda = 1$), a black rectangle shows some regular structure of vortices occurring around the region along the x axis. In fact, they are essentially vortex clusters which degenerate into a line. The number of vortices in each column is the same as that of the cluster in Fig. 2(a). The dual SOC leads the vortices to occur along the x axis, but the repulsion among vortices squeezes them to distribute in a line. Thus, several lines of vortices form a 2D lattice. In the periphery of the lattice there are the remaining vortex clusters. Outside the BECs, the vortices fail to form the full vortex clusters, because the phase separation causes some components to disappear locally. When the strength of the dual SOC increases up to $\lambda = 2$, the structure of the vortices lattice [a black rectangle region in

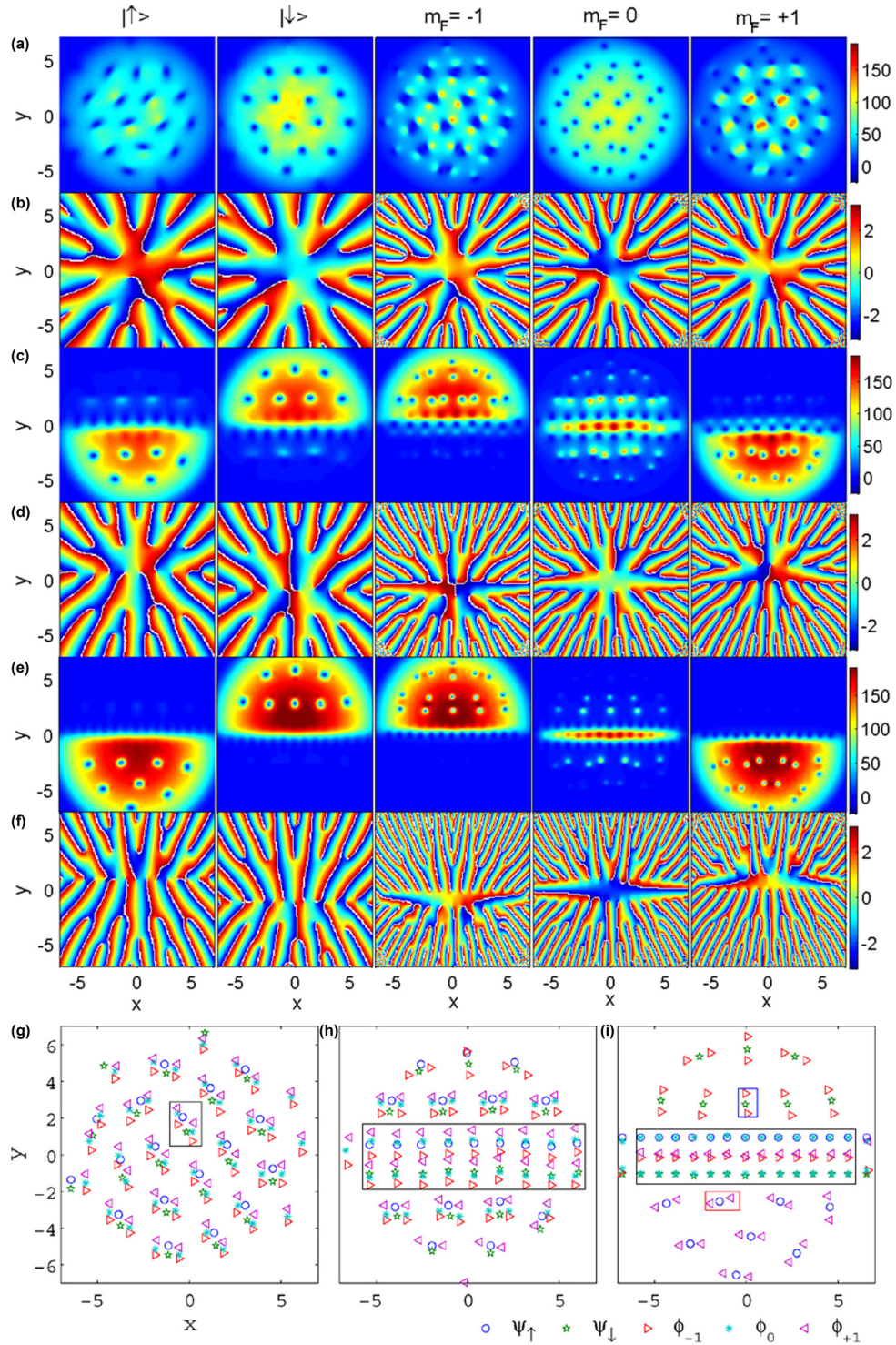


FIG. 3. The effect of dual SOC on the vortices in rotating atomic-molecular BECs. The rotation frequency is $\Omega_{\text{rotation}} = 0.5\omega$, where $\omega = 200 \times 2\pi$ Hz. We set the parameters $g_{\uparrow,\downarrow} = g_{\uparrow,\downarrow} = g_A$ with the scattering length $a_A = 101.8a_B$, $g_{\downarrow,\downarrow} = 0.95g_A$, $g_{AM} = 0.5g_A$, $g_n = 2g_A$, $g_s = 0.03g_A$, $\chi = 0.08$, $\varepsilon = 0$, $\Omega_A = 0.8$, and $\mu_m = 2\mu_a = 3.5\mu_{m,0} = 7\mu_{a,0} = 42\hbar\omega$. (a) Densities of each components under the equilibrium state, the strength of dual SOC $\lambda = 0$. Note that the components are pointed out by the title: $|\uparrow\rangle$, $|\downarrow\rangle$, $m_F = -1$, $m_F = 0$, and $m_F = +1$, respectively. (b) The corresponding phases of each components in (a). [(c) and (d)] The corresponding densities and phases with $\lambda = 1$. [(e) and (f)] The corresponding densities and phases with $\lambda = 2$. [(g) and (i)] The position of vortices in (a), (c), and (e), respectively. In (g), the rectangle points out a vortex cluster. In (h), the rectangle points out the region where the vortices form a lattice. In (i), the red (blue) rectangle marks out a carbon dioxide vortex, and the black rectangle points out the vortices lattice. The particles number $(N_{\uparrow}, N_{\downarrow}, N_{-1}, N_0, N_{+1})$ for the three cases are $(5.82 \times 10^3, 8.01 \times 10^3, 4.96 \times 10^3, 8.23 \times 10^3, 4.93 \times 10^3)$, $(7.86 \times 10^3, 8.80 \times 10^3, 7.95 \times 10^3, 3.93 \times 10^3, 7.85 \times 10^3)$, and $(11.42 \times 10^3, 12.29 \times 10^3, 10.03 \times 10^3, 2.00 \times 10^3, 10.04 \times 10^3)$, respectively. The unit of length, strength of χ , Ω_A , and dual SOC are $0.76 \mu\text{m}$, $\hbar\omega$, ω , and 0.96×10^{-3} m/s, respectively.

Fig. 3(i)] differs from that in Fig. 3(h). Here each vortex of ϕ_0 component tends to overlap with an atomic vortex. The vortex number of ϕ_{+1} (ϕ_{-1}) component decreases to 1 in each column. The blue rectangle and the red rectangle in Fig. 3(i) indicate that vortices form some carbon dioxide structures far from the center of the vortex lattice (black rectangle). Above the black rectangle, vortices in components of ψ_{\downarrow} and ϕ_{-1} form the carbon dioxide structure, whereas the atomic vortex situates in the middle, and two molecular vortices locate at the two sides symmetrically. Similarly, the carbon dioxide structure of vortices in components of ψ_{\uparrow} and ϕ_{+1} occurs below the black rectangle. These results indicate that the strong dual SOC deepens the phase separation. At the same time, it forces the vortices cluster to transform into the lattice around the x axis and even into the carbon dioxide structures in the remaining regions.

We now discuss the effect of the dual SOC on the spin textures. Figures 4(a) and 4(d) show the spin textures in atomic BECs and molecular BECs without dual SOC ($\lambda = 0$), respectively. The topological charge density in Fig. 5(a) [Fig. 5(d)] shows that they are skyrmions (half-skyrmions) with $Q = -1$ ($Q = -\frac{1}{2}$). The position of vortices proves that the skyrmions (half-skyrmions) originate from the vortices dipole of atomic BECs (the three vortices structure of molecular BECs). The sum of topological charge density in Fig. 5(g) indicates that the skyrmion of atomic BECs and the half-skyrmion of molecular BECs form the carbon dioxide structure, which is marked by the blue ellipses.

The dual SOC can redistribute the carbon-dioxide-like skyrmions in the atomic-molecular BECs. For $\lambda = 1$, we also obtain some skyrmions and half-skyrmions in the atomic BECs and molecular BECs, respectively. Due to the phase separation caused by the dual SOC and rotation, some skyrmions are forced to distribute along the x axis in Fig. 4(b). Similarly, some half-skyrmions distribute parallel along the x axis in Fig. 4(e). The topological charge density in Figs. 5(b), 5(e), and 5(h) shows the carbon-dioxide-like skyrmions distribute into a line along the x axis. In other words, the dual SOC induces a chain of carbon-dioxide-like skyrmions.

The strong dual SOC can even redesign the spin excitations of the textures. When the strength of the dual SOC λ reaches 2, the skyrmion can occur in the atomic BECs [see Figs. 4(c) and 5(c)]. The skyrmion along the x axis is induced by the vortices dipole, but the skyrmion away from the x axis is induced by a single vortex. In the molecular BECs, the half-skyrmion is induced by a single vortex of ϕ_{-1} component in the region of $y > 1.5$ [see Figs. 4(f) and 5(f)]. The sum of the topological charge density in Fig. 5(i) further proves that the carbon-dioxide-like skyrmion indeed occurs in the region of $y > 1.5$ and $y < -1.5$. Along the x axis (between the black lines), the spin texture transforms into a structure with a fractional topological charge. This structure is not constructed by the normal half-skyrmion because the singular points in the topological charge densities disappear. Therefore, the extremely strong dual SOC can destroy the half-skyrmion excitations in the original chain of carbon-dioxide-like skyrmions.

Why do the carbon-dioxide-like skyrmions form only one chain? Initially, the atomic-molecular BECs are miscible. Under combined interaction of the rotation and dual SOC, the

phase separation occurs. Around the domain wall, the energy of interaction is lower than that in other parts. Thus, the vortices and the corresponding skyrmions tend to distribute along the domain wall to form the ordered structure. Meanwhile, there is only one domain wall formed when the BECs separate. Therefore, there are no vortices lattices or a chain of carbon-dioxide-like skyrmions in other parts of the BECs.

E. Chern number indicates that spin-orbit coupling induces topological excitations in high- $|k|$ region

Chern number is one of the most canonical topological invariant characterizations. The topological properties can be understood in terms of the Chern number [56] in k space, which is defined as

$$C_{\delta} = \frac{1}{2\pi i} \int \int A_{\delta} d^2k, \quad (5)$$

$$A_{\delta} = i(\langle \partial_{k_x} u_{\delta} | \partial_{k_y} u_{\delta} \rangle - \langle \partial_{k_y} u_{\delta} | \partial_{k_x} u_{\delta} \rangle),$$

where A_{δ} is the Berry curvature and $u_{\delta} = \frac{\phi(k, \delta)}{|\phi(k, \delta)|}$ with the k -space occupied state $\phi(k, \delta)$. Because BECs are described by the macroscopic wave functions of the lowest energy, δ only denotes the corresponding ground states. Here we consider the five components of the spin-dependent atomic-molecular BECs. For example, the k -space occupied state of the ϕ_m ($m = -1, 0, 1$) component is $\phi(k, \delta)$, where $\phi(k, \delta) = FFT(\phi_m)$. We use the $\phi(k, \delta)$ of each component to obtain the corresponding Berry curvature and Chern number.

Figures 6(a)–6(c) show the values of Chern number as $|k|$ increases, where $|k| = \sqrt{k_x^2 + k_y^2}$. These figures correspond to the three cases in Fig. 4. The ladderlike changes of the Chern number mean the variation of the number of topological excitations in k space as the integral radius increases. The platform denotes that there is no change as $|k|$ varies. Finally, the Chern number tends to be some invariants up to 10 or more as $|k|$ is large enough. The topological properties of the system in Figs. 6(a)–6(c) differ considerably from each other because the final Chern numbers which imply the number of topological excitations in k space differ. Additionally, the bottom inset in Fig. 6(a) is A_{\uparrow}/i in k space, where A_{\uparrow} is the Berry curvature of ψ_{\uparrow} . Obviously, most of its value is 0, except some points whose values are up to thousands. These points almost are discretely and equally distributed around the position (0,0). Thus, the topological excitations have different momentums in k space. This phenomenon is easy to be understood because the topological excitations tend to occur with the momentum as low as possible. Meanwhile, the topological excitations also have a nonzero size and have the interaction with each other in k space, which lead to the discrete distribution. When SOC increases to $\lambda = 1$, the points almost separate into two parts. One part is in $k_x > 0.5$ and the other is in $k_x < -0.5$, while there is no points around the region of k_y axis. The number of points in the region of $k_x < -0.5$ is much more than that in the region of $k_x > 0.5$ [see the inset in Fig. 6(b)]. This indicates that the topological excitations with k_x around 0 are restrained by SOC. And they have to get a higher momentum of k_x . Thus, the topological excitations have to get together along the x direction. This is a main reason for the creation of topological spin textures's chain in Figs. 4

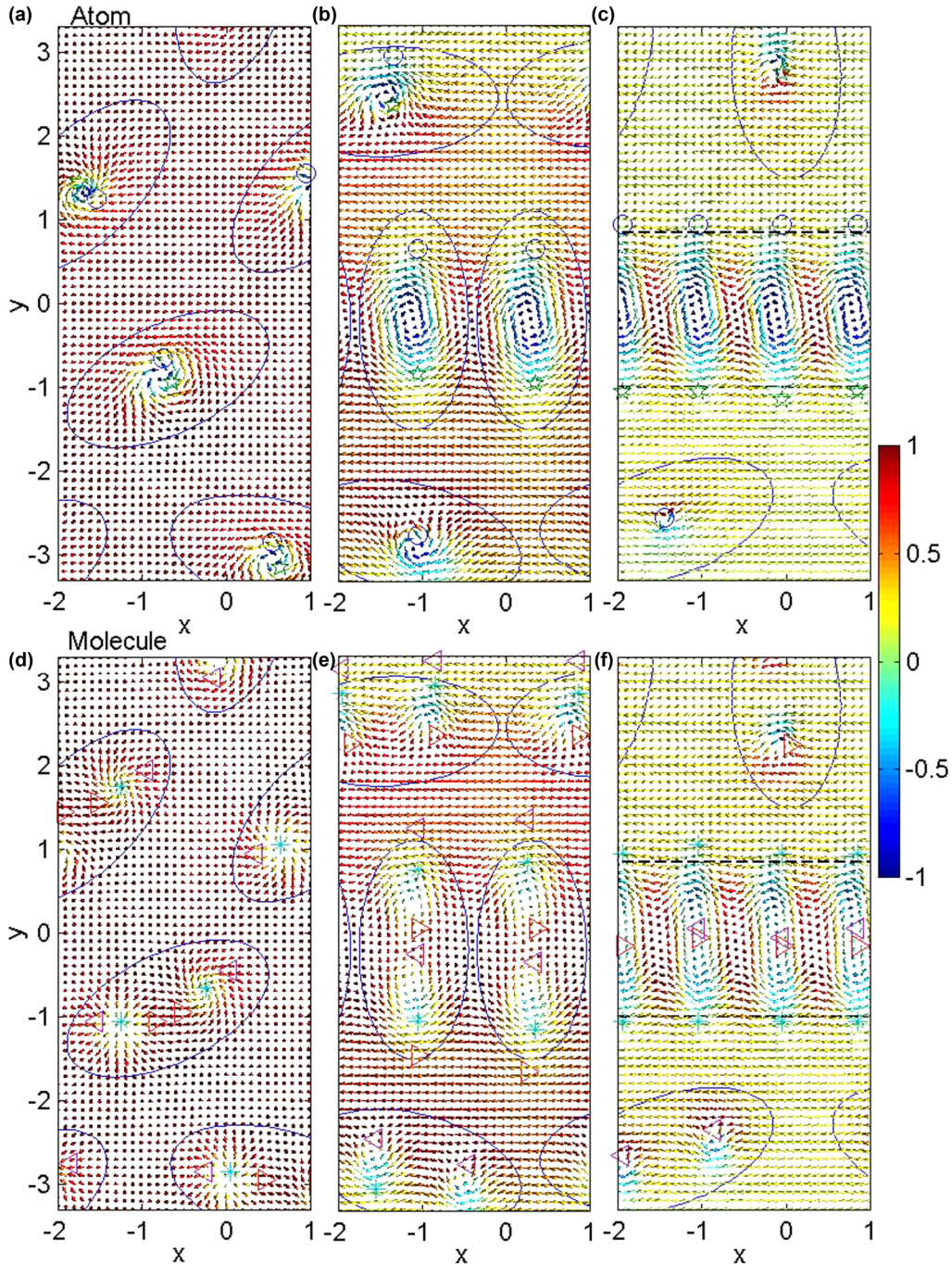


FIG. 4. The effect of SO coupling on the spin texture in the atomic-molecular BECs. [(a)–(c)] The corresponding spin textures of atomic BECs in Figs. 3(a), 3(c), and 3(e), respectively. [(d)–(f)] The corresponding spin textures of molecular BECs in Fig. 3(a), 3(c), and 3(e), respectively. Note that the spin textures are under the transformation: $(S'_x, S'_y, S'_z) = (S_z, S_y, -S_x)$. The color of each arrow indicates the magnitude of S'_z . The blue ellipses point out the regions of the carbon-dioxide-type skyrmion that skyrmion of atomic BECs couples two half-skyrmion of molecular BECs. In addition, we mark the position of vortices in order to illuminate the relationship between spin texture and position of vortices clearly. The meanings of the marks are the same as that in Figs. 3(g)–3(i). The unit of length, strength of χ , Ω_A , and SO coupling are $0.76 \mu\text{m}$, $\hbar\omega$, ω , and $0.96 \times 10^{-3} \text{ m/s}$, respectively.

and 5. Therefore, SOC changes the properties of topological excitations according to the momentum. When SOC is up to $\lambda = 2$, almost all the points are in the region of $k_x > 1.5$ [see the inset in Fig. 6(c)]. In this case, the topological spin textures form a more serried chain.

We can define three parameters K_a , K_m , and K_{\min} to characterize the properties of topological excitations represented by Chern number. K_a is the average position of the first hop of Chern number in atomic BECs with ψ_\uparrow and ψ_\downarrow . Similarly, K_m is that in molecular BECs with ϕ_{+1} and ϕ_{-1} , and K_{\min}

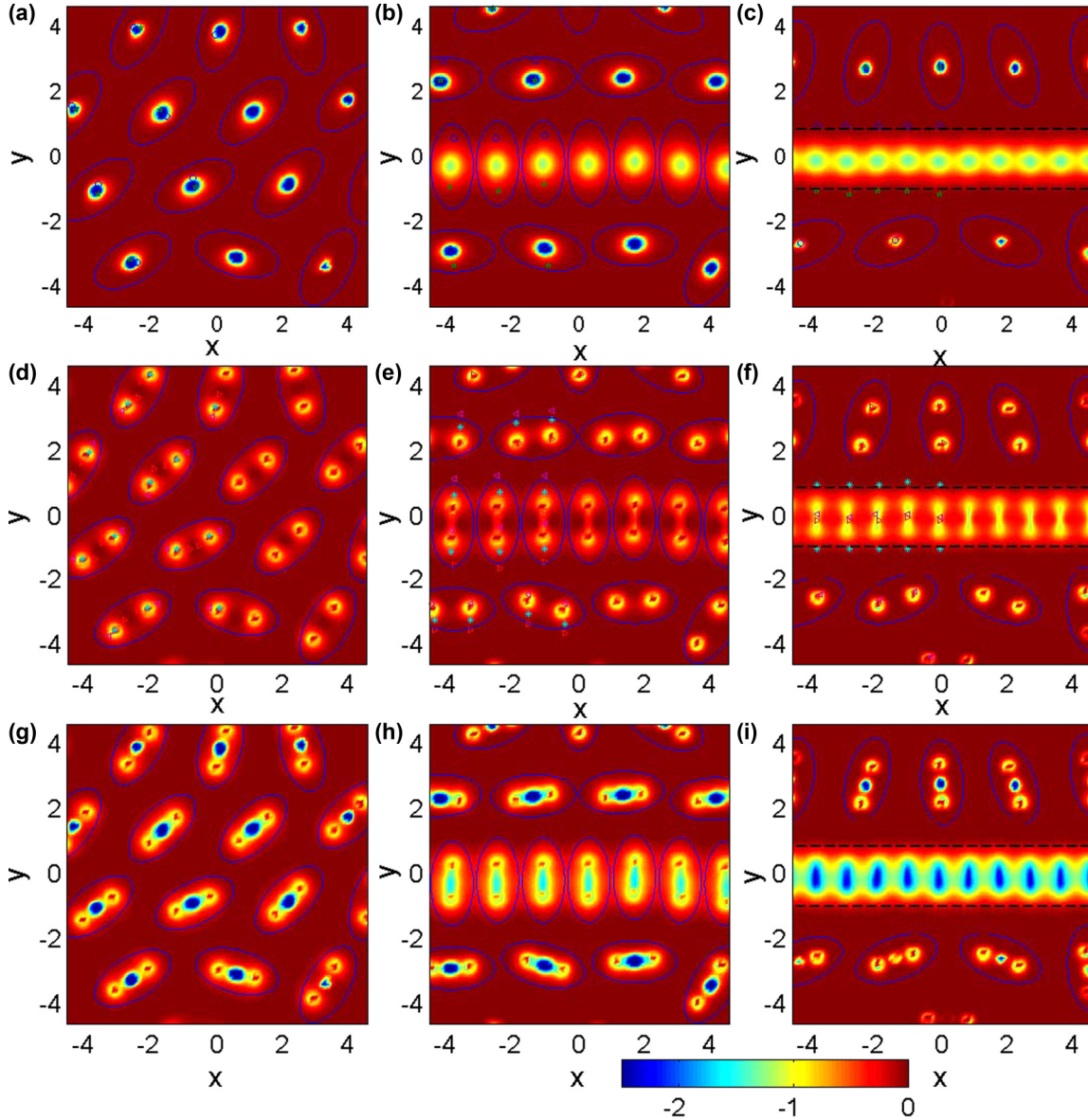


FIG. 5. The topological charge density of spin textures in SO coupled atomic-molecular BECs. [(a)–(c)] The corresponding topological charge density in Fig. 4(a)–4(c), respectively. [(d)–(f)] The corresponding topological charge density in Figs. 4(d)–4(f), respectively. In addition, we mark the position of vortices in $x < 0$ region in order to illuminate the relationship between spin texture and position of vortices clearly. The meanings of the marks are the same as that in Figs. 3(g)–3(i). [(g)–(i)] The total topological charge density of (a) and (d), (b) and (e), and (c) and (f), respectively. We use the blue ellipses to point out the regions of the carbon-dioxide-type skyrmion. The unit of length and SO coupling are $0.76 \mu\text{m}$ and $0.96 \times 10^{-3} \text{ m/s}$, respectively.

is the minimum value of the first hop of the Chern number in the whole atomic-molecular BECs. Comparing these three cases, we find that the values of K_a (K_m , K_{\min}) are the largest in Fig. 6(c), the middle in Fig. 6(b), and the least in Fig. 6(a) (see the top inset). These phenomena further show that SOC forces the Chern number to be induced in the high- $|k|$ region and restrain it in the low- $|k|$ region.

Figure 6(d) shows the value of Chern number as a function of SOC. SOC changes the topological properties of the whole system because the values of Chern number depend on it. SOC would finally restrict the Chern number when SOC is strong enough, but SOC can not restrict its value to be zero

completely. We also examine the value of $\langle C(k) \times k^2 \rangle$ in Fig. 6(e) and $\langle C(k) \times k^2 \rangle / \langle C(k) \rangle$ in Fig. 6(f). $\langle C(k) \times k^2 \rangle$ implies the total properties of energy of all topological excitations in the system, while $\langle C(k) \times k^2 \rangle / \langle C(k) \rangle$ implies the average properties. Figure 6(f) shows that the value of $\langle C(k) \times k^2 \rangle / \langle C(k) \rangle$ tends to become larger as SOC increases. Thus, the topological excitations which are characterized by the Chern number should be induced in the high- $|k|$ region. Therefore, SOC plays a role in changing energy of the topological excitations. With the application of SOC, we can have the separated carbon-dioxide-like skyrmions construct as the chain, whose energy is obviously much higher than the former.

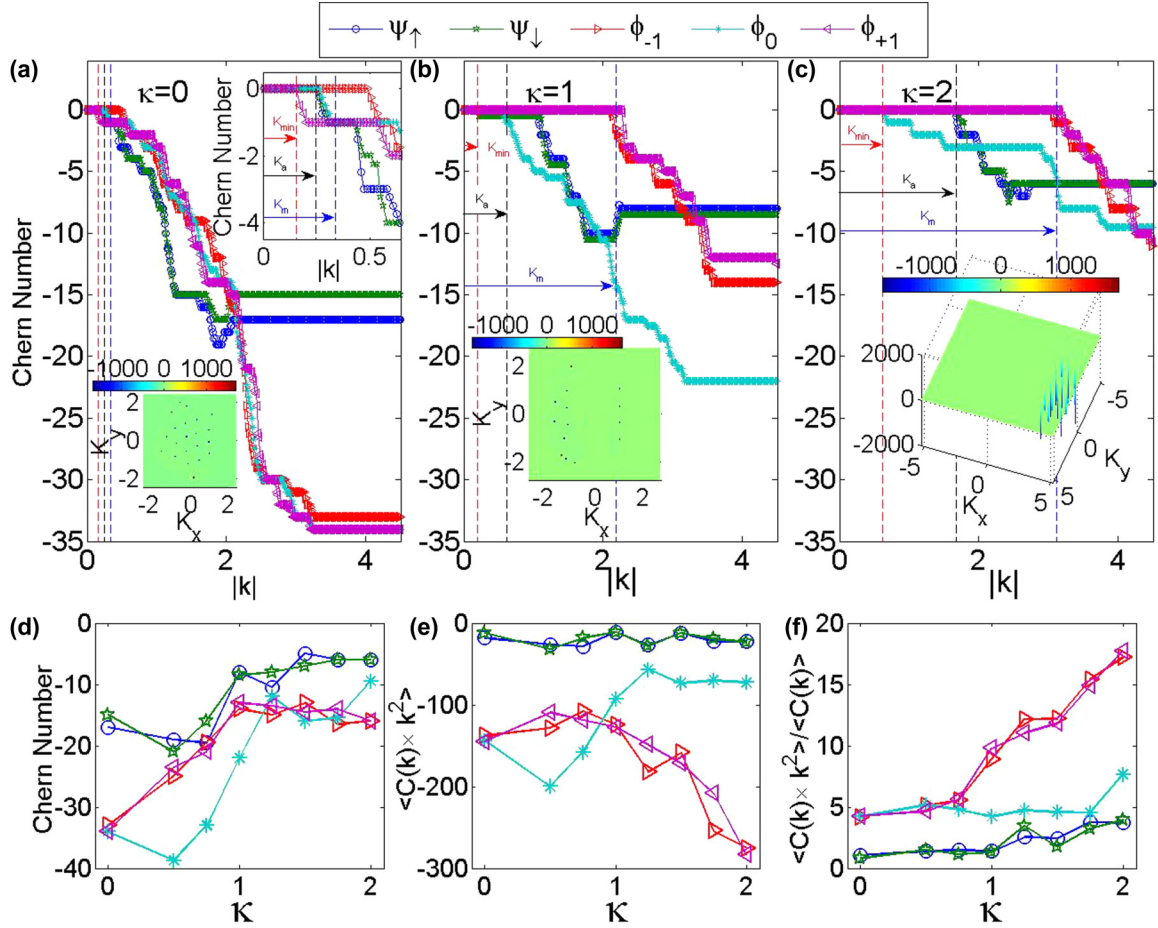


FIG. 6. Chern number verifying the high- $|k|$ topological excitations in the dual SOC atomic-molecular BECs. [(a)–(c)] Chern number in k space of atomic-molecular BECs in Figs. 3(a), 3(c), and 3(e), respectively. The top inset in Fig. 6(a) is a local enlargement. The red dotted line and the red arrow indicate the minimum value K_{\min} for the first hop as $|k|$ increases. The black dotted line and black arrow show the first hop of average position K_a in atomic BECs of ψ_\uparrow and ψ_\downarrow . Similarly, the blue dotted line and blue arrow show the first hop of average value K_m in molecular BECs of ϕ_{+1} and ϕ_{-1} . The bottom inset in Fig. 6(a) is A_\uparrow/i under $\lambda = 0$, where A_\uparrow is the Berry curvature of ψ_\uparrow . Similarly, the inset in Fig. 6(b) is A_\uparrow/i under $\lambda = 1$. The inset in Fig. 6(c) is A_{-1}/i under $\lambda = 2$. (d) Chern number as function of strength of SOC λ . (e) $\langle C(k) \times k^2 \rangle$ as function of strength of SOC λ . (f) $\langle C(k) \times k^2 \rangle / \langle C(k) \rangle$ as function of strength of SOC λ .

F. Phase diagram of the topological spin textures in the spin-orbit coupled atomic-molecular BECs

Figure 7 plots the phase diagrams of the SOC atomic-molecular BECs with various products in our numerical simulations. In Fig. 7(a), there is no skyrmion excitations when the rotation frequency is very low (see the red region). The white region shows the occurrence of only a single carbon-dioxide-like skyrmion. As long as the rotation frequency is not too low, the skyrmion excitations appear. The induced carbon-dioxide-like skyrmions are separated when SOC is very weak (see the magenta region). At the yellow region, we can obtain the chain formed by carbon-dioxide-like skyrmions across the BECs. If SOC is strong enough (see the green region), then the half-skyrmions attached to the center skyrmion chain would be destroyed.

We further examine the effect of the interaction g_{am} on the products with a fixed rotation frequency $\Omega_{\text{rotation}} = 0.5\omega$ in Fig. 7(b). Similarly, as its strength increases, SOC can make the products be separated carbon-dioxide-like skyrmion (see

the magenta region), the carbon-dioxide-like skyrmion chain (see the yellow region), and the destroyed half-skyrmions (see the green region), respectively. However, if g_{am}/g_a is larger than 1.1, then the phase separation destroys the combinations among the topological excitations. So we only obtain the separated skyrmions and half-skyrmions.

II. DISCUSSION

First, we discuss the feasibility of our schematic. For creating molecule BEC, some previous studies [57–59] have shown that direct conversion via Raman photoassociation [3–8] is feasible. Under this mechanism, the pairs of atoms from the two-atom continuum of the ground electronic potential are transferred via an excited bound molecular state to a bound molecular state of a lower energy in the ground potential. Raman photoassociation allows coupling to a single molecular state, which can be selected by the Raman laser frequencies. However, practical estimates using

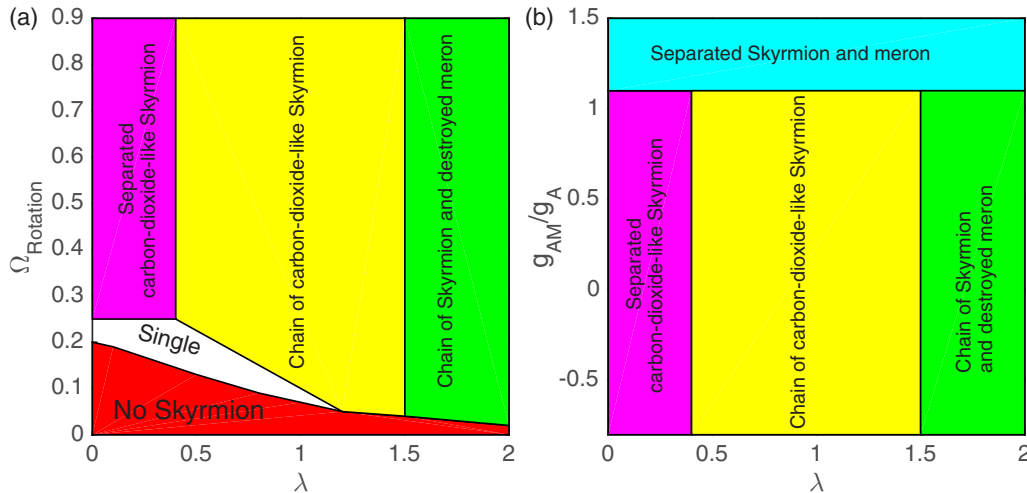


FIG. 7. Phase diagram of topological spin textures in the dual SOC atomic-molecular BECs. (a) Ration frequency-SOC ($\Omega_{\text{rotation}} - \lambda$) phase diagram for the products. We set the parameters $\omega = 200 \times 2\pi$ Hz, $\chi = 0.03$, $\Omega_A = 0.8$, $g_{\uparrow,\downarrow} = g_A$ with the scattering length $a_A = 101.8a_B$, $g_{\downarrow,\downarrow} = 0.95g_A$, $g_n = 2g_A$, $g_s = 0.03g_A$, $g_{AM} = 0.5g_A$, $\varepsilon = 0$ and $\mu_m = 2\mu_a = 3.5\mu_{m,0} = 7\mu_{a,0} = 28\hbar\omega$. (b) Atom-molecule interaction-SOC [$(g_{AM}/g_A) - \lambda$] phase diagram for the products. We set the parameters $\omega = 200 \times 2\pi$ Hz, $\chi = 0.03$, $\Omega_A = 0.8$, $g_{\uparrow,\downarrow} = g_{\downarrow,\downarrow} = g_A$ with the scattering length $a_A = 101.8a_B$, $g_{\downarrow,\downarrow} = 0.95g_A$, $g_n = 2g_A$, $g_s = 0.03g_A$, $\varepsilon = 0$, and $\mu_m = 2\mu_a = 3.5\mu_{m,0} = 7\mu_{a,0} = 28\hbar\omega$. The unit of length, strength of χ , Ω_A , and SOC are $0.76 \mu\text{m}$, $\hbar\omega$, and 0.96×10^{-3} m/s, respectively.

available lasers and transitions indicate that coherent transfer may be limited by spontaneous emission from the intermediate molecular excited electronic state. In addition, realistic analysis and experimental implementations indicate that the loss processes due to inelastic atom-molecule collisions occur at a significant rate [60–62]. How do we solve the problems coming from spontaneous emission and inelastic atom-molecule collisions? A possible route towards minimizing losses and decoherence from spontaneous emission in photoassociation is the stimulated Raman adiabatic passage [62,63], in which a counterintuitive pulse sequence is used, where the first input pulse couples the molecular levels even when there are no molecules present. In this situation, a dark superposition state is formed, due to interference effects between the atomic and molecular electronic ground states. This minimizes the probability of a real transition to the molecular excited state and hence reduces spontaneous emission.

We now give an outlook for the future experiment about atomic-molecular BECs. In this study, our schematic has only shown a possible method for the creation of dual SOC atomic-molecular BECs. In the real experiments, the realization of dual SOC atomic-molecular BECs would be affected by lots of factors such as spontaneous Raman scattering by molecules [60–62], the inelastic collision channels between atoms and molecules [4], heating due to spontaneous scattering, some undesired light shifts [4,6], and inhomogenous detuning of the laser fields. In this work, we do not solve all the problems, but we attempt to give an outlook for future work, which would guide the interested researchers. It includes the following items for BECs' experiments as follows:

(i) Although coherent coupling between the atomic and molecular BEC has been realized in experiment [4,5], whether a coherent atomic-molecular dressed state can be sustained needs experimental verification.

(ii) Rotationally or vibrationally inelastic atom-molecule collisions may exist in this system [4]. How to solve inelastic collision channels between atoms and molecules is an important question.

(iii) It is well known that heating due to spontaneous scattering is already a serious limitation on SOC with atomic BECs involving two lasers [10–15]. How to solve heating due to spontaneous scattering is a very common question in future works.

(iv) The (elastic) scatterings [3] are unlikely to be all equal, and it likely that this will have a significant impact on miscibility of the components. How do the scattering properties affect the SOC effect?

(v) Light shifts will greatly affect the characterizing equations [4,6]. How do we avoid some undesired light shifts when there are lots of lasers in the experiments?

(vi) When the two-photon linewidths are small, mean-field shifts [64] would cause spatially inhomogenous detuning of the laser fields. How do we avoid this effect?

Solutions to these potential issues could dramatically improve our current experimental techniques for ultracold atoms and molecules.

In the Supplemental Material [55], we further prove that Raman coupling enhances the creation of carbon-dioxide-like skyrmion and chain (see Figs. S1, S2, S3, S4, and S5 in the Supplemental Material [55]). The case in Fig. 4(a) of single Raman coupling without dual SOC would be realized by lasers with the same direction. It is impossible to only hold the Raman coupling but neglect the dual SOC with the counterpropagating Raman lasers. If the counterpropagating Raman lasers are turned off, i.e., both Raman coupling and dual SOC are terminated, the carbon-dioxide-like skyrmions and the chain do not occur in the rotating atomic-molecular BECs, although the superchemistry

effect is considered (see Figs. S6 in the Supplemental Material [55]). Furthermore, there are no nontrivial spin texture excitations if the rotation frequency decreases to zero. Due to the dependence of the spin-dependent photoassociation and Raman lasers, carbon-dioxide-like skyrmions and the chain are the special phenomena that exist in the rotating dual SOC atomic-molecular BECs with hyperfine spin states.

In this study, we have found that the SOC atom-molecular BECs support large Chern numbers up to 10 or more. We have used the Chern number to analyze the effect of SOC on the topological excitations in atomic-molecular BECs. On the one hand, SOC would change the topological properties according to the value of the Chern number. On the other hand, SOC could effectively suppress the Chern number to be induced in the low- $|k|$ region and promote it to be induced in the high- $|k|$ region. This effect leads to the chainlike reconstruction of topological spin textures. We have first considered the spin of atomic-molecular BECs and given a proposal to create dual SOC in this system. They are important challenges to extend scalar BEC to spinor one and to extend atomic BECs to more complicated atomic-molecular BECs. Similarly, our consideration realizes another challenge to extend normal atomic-molecular BECs to the spinor ones. This untouched system is a new platform for producing SOC and discovering unconventional topological excitations.

Half-skyrmion pairs in our study differ from meron-antimeron ones, whose total topological charge is zero. It is doubtful that the meron (half-skyrmion) pairs are induced by vortices molecule because the topological charge density shows only one center but not two for each meron pairs [50]. Additionally, if we plot the topological charge density with the meron pairs' solution in Ref. [50], we will obtain two centers. One is positive, the other is negative, and the total topological charge is zero. Thus, the solution in Ref. [50] does not match with the properties of meron pairs. skyrmions are often viewed as the ideal information carriers of great prospect in future application via the creation and annihilation [1,2]. The carbon-dioxide-like skyrmion is the result of combining the separated topological excitations to form a structural cell. This property implies that if the carbon-dioxide-like skyrmions can serve as information carriers [1,2], including the creation and annihilation, their distribution in lines one by one, and the combination and separation will demonstrate the potential for information storage. Thus, the carbon-dioxide-like skyrmion allows more complex control than normal skyrmion discussed previously for information carriers.

In the real experiments, the carbon-dioxide-like skyrmion would be identified by direct observation of the densities via a time-of-flight absorption imaging technique [65–67], which can measure the characteristics of the carbon-dioxide-like skyrmion by means of corresponding quantum vortices. The experiments should begin with a nearly pure ^{87}Rb BEC of approximately 3.0×10^5 or more atoms in the $|f = 1, m_f = -1\rangle$ state [10–15]. An initially off-resonant radio-frequency magnetic field can be used to prepare equal mixtures of $|f = 1, m_f = -1\rangle$ and $|f = 1, m_f = 0\rangle$. Then, the spin-dependent photoassociation of atom [39,40] creates the molecules of $|F = 2, m_F = 0, -1, -2\rangle$, which are used to produce the excited molecules of $|F = 1, m_F = 0, \pm 1\rangle$ via the transition

$\Delta F = -1$ and $\Delta m_F = +1$, and, finally, the excited molecules degenerate to be the molecular BECs of $|F = 1, m_F = 0, \pm 1\rangle$ [see Figs. 1(d)–1(f)]. At the same time, the counterpropagating Raman lasers $L3$ and $L4$ ($L5$, $L6$, and $L7$) shown in Fig. 1 are used to induce dual SOC for atomic (molecular) BECs [10–15]. Combining rotation effect and further cooling process, one would obtain the dual SOC atomic-molecular BECs at the equilibrium state. In this study, our results have shown that the carbon-dioxide-like skyrmion is related either to vortices cluster or to carbon-dioxide vortices. The vortex cluster consists of two atomic vortices and six molecular vortices [see the black rectangle in Fig. 4(g)]. Comparing with the structure of vortices cluster, the structure of the carbon-dioxide vortices is simpler [see the red and blue rectangles in Fig. 4(i)]. Therefore, one can apply a ballistic expansion (approximately 20 ms) of the BECs in a gradient magnetic field to separate the different spin states [65–67]. Vortices will be imprinted by ramping the magnetic field $B_z \rightarrow 0$. After the structures of vortices are measured, the carbon-dioxide-like skyrmion can be identified.

In summary, we have constructed an experimental proposal for creating dual SOC in atomic-molecular BECs by combining the spin-dependent photoassociation and Raman coupling. This type of dual SOC can force the Chern number to be induced in the high- $|k|$ region, which finally determines the formation of the topological spin texture excitations. Thus, we not only find that the SOC atomic-molecular BECs support a novel composite topological excitation (the carbon-dioxide-like skyrmion, whose topological charge is -2) but also find that SOC can induce the carbon-dioxide-like skyrmion to link to be polymer chain. This work opens a new window to realize SOC in multicomponent ultracold gases and manipulate complex nontrivial topological excitations in future experiments.

ACKNOWLEDGMENTS

We thank P. Zhang and H. Jing for helpful discussions. C.F.L. is supported by the NSFC under Grants No. 11304130, No. 11365010, No. 61565007; the Jiangxi provincial Department of Science and Technology (Grants No. 20151BAB212002 and No. 20162BCB23049) and the Jiangxi provincial Department of Education (No. GJJ150685); and the Program of Qingjiang Excellent Yong Talents, Jiangxi University of Science and Technology. W.M.L. is supported by the NKRDIP under Grant No. 2016YFA0301500; the NSFC under Grants No. 11434015, No. 61227902, No. 61378017, and No. KZ201610005011; SKLQQOD under Grant No. KF201403; and SPRPCAS under Grants No. XDB01020300 and No. XDB21030300.

APPENDIX

1. The equations of the spin-orbit coupling atomic-molecular BECs

Experimentally, the equal-Rashba-Dresselhaus SOC can be obtained by using the Raman-coupling of two hyperfine states in the ground-state manifold of alkali atoms [10–15]. In that case, the strength of the SOC depends on the wave vectors of

the Raman lasers. On the other hand, the effective out-of-plane (in-plane) Zeeman field is proportional to the Rabi frequency of the Raman process, i.e., to the matrix element of the two-photon coupling between a selected pair of atomic magnetic sublevels of the ground-state manifold. It is well known that the molecular BEC can be created by the Raman photoassociation of atoms in a condensate [3–8]. With the spin-dependent photoassociation [39,40], the hyperfine states of molecules are related to those of the converted atoms. Furthermore, a number of experiments have demonstrated a high degree of control over the hyperfine state of ultracold molecules via two-photon optical Raman transitions [39,40,68,69]. Here, when considering the SOC in atomic-molecular BECs, we are dealing with atoms characterized by two different internal (quasispin) states, as well as molecules with three spin states ($F = 1, m_F = 0, \pm 1$).

The SOC of atomic BECs can be generated by two additional Raman beams (ω_{L3} and ω_{L4}) which couple the atomic internal states $|\uparrow\rangle$ and $|\downarrow\rangle$. The single-atom Hamiltonian induced by the Raman coupling is $\Omega_A |\uparrow\rangle\langle\downarrow| e^{-2ik_x X} + \text{H.c.}$, with Ω_A the atomic Raman coupling intensity. Furthermore, Raman beams (ω_{L5} , ω_{L6} , and ω_{L7}) couple different molecular internal states $|m_F = 0, \pm 1\rangle$ and lead to Hamiltonian ($|m_F = 0\rangle\langle m_F = -1| + |m_F = 1\rangle\langle m_F = 0|$) $\Omega_M e^{ik_x X} + \text{H.c.}$, with X the position of the mass center of the two atoms and $\Omega_M = \sqrt{2}\Omega_A$.

To clearly illustrate effects of the SOC, we introduce a unitary transformation $U_A = e^{i\sigma_z k_x X}$ and $U_M = \sum_{m=0,\pm 1} e^{2imk_x X} |m_F = m\rangle\langle m_F = m|$ for the atomic states and molecular states, respectively, with $\sigma_z = |\uparrow\rangle\langle\uparrow| - |\downarrow\rangle\langle\downarrow|$. Therefore, in the spin-rotated frame induced by a combined transformation $U = U_A P^A + U_M P^M$, the Hamiltonian is $H = U H' U^\dagger$, where H' is the Hamiltonian in the original (unrotated) frame, P^A and P^M being the projection operators onto the atomic and molecular states. A straightforward calculation shows that, for the condensate in the d -dimensional space ($d = 1, 2, 3$), in the second quantization we have

$$H = H_{AF} + H_{MF} + H_{\text{SOC}} + H_{\text{Raman}} + H_{AM} + H_I. \quad (\text{A1})$$

Here $H_{AF} = \sum_{a=\uparrow,\downarrow} \int \hat{\psi}_a^\dagger(\vec{r}) [-\hbar^2 \nabla_d^2 / (2M_A) + M_A \omega^2 r^2 / 2] \hat{\psi}_a(\vec{r}) d\vec{r}$ and $H_{MF} = \sum_{m=0,\pm 1} \int \hat{\phi}_m^\dagger(\vec{r}) [-\hbar^2 \nabla_d^2 / (4M_A) + M_A \omega^2 r^2 + \varepsilon + M_A \lambda^2 m^2] \hat{\phi}_m(\vec{r}) d\vec{r}$ are the free Hamiltonians for atoms and molecules, respectively, where M_A is the single-atom mass, ω is the trapping frequency, ε is the difference between the binding energy to the two-atom molecule and the frequency difference of the two laser beams which induce atom-molecule coupling, the factor λ is defined as $\lambda = k_x / M_A$, the operator $\hat{\psi}_a^\dagger(\vec{r})$ ($a = \uparrow, \downarrow$) is the creation operator for a single atom at position \vec{r} with internal state $|a\rangle$, and $\hat{\phi}_m^\dagger(\vec{r})$ ($m = 0, \pm 1$) is the creation operator for a single molecular at position \vec{r} with internal state $|m_F = m\rangle$.

In Eq. (A1) the SOC is described by

$$\begin{aligned} H_{\text{SOC}} = & \lambda \int \hat{\psi}_\uparrow^\dagger(\vec{r}) (-i\hbar \partial_x) \hat{\psi}_\uparrow(\vec{r}) d\vec{r} \\ & - \lambda \int \hat{\psi}_\downarrow^\dagger(\vec{r}) (-i\hbar \partial_x) \hat{\psi}_\downarrow(\vec{r}) d\vec{r} \\ & + \lambda \int \hat{\phi}_1^\dagger(\vec{r}) (-i\hbar \partial_x) \hat{\phi}_1(\vec{r}) d\vec{r} \\ & - \lambda \int \hat{\phi}_{-1}^\dagger(\vec{r}) (-i\hbar \partial_x) \hat{\phi}_{-1}(\vec{r}) d\vec{r}. \end{aligned}$$

The Raman coupling between internal states is described by

$$\begin{aligned} H_{\text{Raman}} = & \Omega_A \int \hat{\psi}_\uparrow^\dagger(\vec{r}) \hat{\psi}_\downarrow(\vec{r}) d\vec{r} + \Omega_M \int \hat{\phi}_1^\dagger(\vec{r}) \hat{\phi}_0(\vec{r}) d\vec{r} \\ & + \Omega_M \int \hat{\phi}_0^\dagger(\vec{r}) \hat{\phi}_{-1}(\vec{r}) d\vec{r} + \text{H.c.} \end{aligned}$$

The laser-induced atom-molecule transition is described by

$$\begin{aligned} H_{AM} = & \chi \int d\vec{r} [\hat{\psi}_\uparrow^\dagger(\vec{r}) \hat{\phi}_\uparrow^\dagger(\vec{r}) / \sqrt{2} + \hat{\psi}_\downarrow^\dagger(\vec{r}) \hat{\phi}_\uparrow(\vec{r}) \hat{\phi}_\downarrow(\vec{r}) \\ & + \hat{\psi}_{-1}^\dagger(\vec{r}) \hat{\phi}_\downarrow^\dagger(\vec{r}) / \sqrt{2} + \text{H.c.}]. \end{aligned}$$

In our system the interparticle interaction is described by H_I in Eq. (A1), and we have $H_I = U_{AA} + U_{AM} + U_{MM}$. Here $U_{AA} = \sum_{a=\uparrow,\downarrow} g_{aa} \int d\vec{r} \hat{\psi}_a^\dagger(\vec{r})^2 \hat{\psi}_a(\vec{r})^2 / 2 + g_{\uparrow\downarrow} \int d\vec{r} \hat{\psi}_\uparrow^\dagger(\vec{r}) \hat{\psi}_\downarrow^\dagger(\vec{r}) \hat{\psi}_\downarrow(\vec{r}) \hat{\psi}_\uparrow(\vec{r})$ describes the atom-atom collision, $U_{AM} = \sum_{a=\uparrow,\downarrow} \sum_{m=0,\pm 1} g_{am} \int d\vec{r} \hat{\psi}_a^\dagger(\vec{r}) \hat{\phi}_m^\dagger(\vec{r}) \hat{\phi}_m(\vec{r}) \hat{\psi}_a(\vec{r})$ describes the atom-molecule collision, and U_{MM} describes the molecule-molecule collision. In the usual case the collisions between molecules with different internal states are quite complicated. Here, for simplicity, we assume in our system the scattering of three-component molecules has the same property as the scattering of $F = 1$ atoms [70,71], i.e., the scattering amplitude is totally determined by the total spin of the two molecules. In that case, we have

$$\begin{aligned} U_{MM} = & \sum_{m,m'=0,\pm 1} \int d\vec{r} \left[\frac{g_n}{2} \hat{\phi}_m^\dagger(\vec{r}) \hat{\phi}_{m'}^\dagger(\vec{r}) \hat{\phi}_{m'}(\vec{r}) \hat{\phi}_m(\vec{r}) \right] \\ & + \sum_{\alpha=x,y,z} \sum_{m,n,k,l=0\pm 1} \int d\vec{r} \left[\frac{g_s}{2} \hat{\phi}_k^\dagger(\vec{r}) \hat{\phi}_n^\dagger(\vec{r}) \right. \\ & \left. \times (F_\alpha)_{nm} (F_\alpha)_{kl} \hat{\phi}_m(\vec{r}) \hat{\phi}_l(\vec{r}) \right]. \end{aligned}$$

In this way, we obtain the coupled equations of the atomic-molecular BECs with dual SOC. It can be written as

$$\begin{aligned} i\hbar \frac{\partial \psi_\uparrow}{\partial t} = & \left[-\frac{\hbar^2 \nabla_d^2}{2M_A} + \frac{M_A \omega^2 r^2}{2} \right] \psi_\uparrow + \lambda p_x \psi_\uparrow + \hbar \Omega_A \psi_\downarrow + \left(\sum_{a=\uparrow,\downarrow} g_{\uparrow,a} |\psi_a|^2 + \sum_{m=0,\pm 1} g_{\uparrow,m} |\phi_m|^2 \right) \psi_\uparrow \\ & + (\sqrt{2} \chi \psi_\uparrow^* \phi_{+1} + \chi \psi_\uparrow^* \phi_0), \end{aligned} \quad (\text{A2})$$

$$i\hbar \frac{\partial \psi_{\downarrow}}{\partial t} = \left[-\frac{\hbar^2 \nabla_d^2}{2M_A} + \frac{M_A \omega^2 r^2}{2} \right] \psi_{\downarrow} - \lambda p_x \psi_{\downarrow} + \hbar \Omega_A \psi_{\uparrow} + \left(\sum_{a=\uparrow, \downarrow} g_{\downarrow, a} |\psi_a|^2 + \sum_{m=0, \pm 1} g_{\downarrow, m} |\phi_m|^2 \right) \psi_{\downarrow} + (\sqrt{2} \chi \psi_{\downarrow}^* \phi_{-1} + \chi \psi_{\uparrow}^* \phi_0), \quad (\text{A3})$$

$$i\hbar \frac{\partial \phi_{+1}}{\partial t} = \left[-\frac{\hbar^2 \nabla_d^2}{2M_M} + \frac{M_M \omega^2 r^2}{2} \right] \phi_{+1} + \frac{\chi}{\sqrt{2}} \psi_{\uparrow}^2 + (\varepsilon + M_A \lambda^2) \phi_{+1} + \lambda p_x \phi_{+1} + \sqrt{2} \hbar \Omega_A \phi_0 + \left(\sum_{a=\uparrow, \downarrow} g_{a, +1} |\psi_a|^2 + g_n \sum_{m=0, \pm 1} |\phi_m|^2 \right) \phi_{+1} + g_s (|\phi_{+1}|^2 + |\phi_0|^2 - |\phi_{-1}|^2) \phi_{+1} + g_s \phi_{-1}^+ \phi_0 \phi_0, \quad (\text{A4})$$

$$i\hbar \frac{\partial \phi_0}{\partial t} = \left[-\frac{\hbar^2 \nabla_d^2}{2M_M} + \frac{M_M \omega^2 r^2}{2} \right] \phi_0 + \chi \psi_{\uparrow} \psi_{\downarrow} + \varepsilon \phi_0 + \sqrt{2} \hbar \Omega_A (\phi_{+1} + \phi_{-1}) + \left(\sum_{a=\uparrow, \downarrow} g_{a, 0} |\psi_a|^2 + g_n \sum_{m=0, \pm 1} |\phi_m|^2 \right) \phi_0 + g_s (|\phi_{+1}|^2 + |\phi_{-1}|^2) \phi_0 + 2g_s \phi_0^+ \phi_{+1} \phi_{-1}, \quad (\text{A5})$$

$$i\hbar \frac{\partial \phi_{-1}}{\partial t} = \left[-\frac{\hbar^2 \nabla_d^2}{2M_M} + \frac{M_M \omega^2 r^2}{2} \right] \phi_{-1} + \frac{\chi}{\sqrt{2}} \psi_{\downarrow}^2 + (\varepsilon + M_A \lambda^2) \phi_{-1} - \lambda p_x \phi_{-1} + \sqrt{2} \hbar \Omega_A \phi_0 + \left(\sum_{a=\uparrow, \downarrow} g_{a, -1} |\psi_a|^2 + g_n \sum_{m=0, \pm 1} |\phi_m|^2 \right) \phi_{-1} + g_s (|\phi_{-1}|^2 + |\phi_0|^2 - |\phi_{+1}|^2) \phi_{-1} + g_s \phi_{+1}^+ \phi_0 \phi_0. \quad (\text{A6})$$

-
- [1] N. Romming, C. Hanneken, M. Menzel, J. E. Bickel, B. Wolter, K. von Bergmann, A. Kubetzka, and R. Wiesendanger, *Science* **341**, 636 (2013).
- [2] N. Nagaosa and Y. Tokura, *Nat. Nano.* **8**, 899 (2013).
- [3] R. Wynar, R. S. Freeland, D. J. Han, C. Ryu, and D. J. Heinzen, *Science* **287**, 1016 (2000).
- [4] D. J. Heinzen, R. Wynar, P. D. Drummond, and K. V. Kheruntsyan, *Phys. Rev. Lett.* **84**, 5029 (2000).
- [5] E. A. Donley, N. R. Claussen, S. T. Thompson, and D. E. Weiman, *Nature (London)* **417**, 529 (2002).
- [6] C. McKenzie, J. Hecker Denschlag, H. Häffner, A. Browaeys, L. E. E. de Araujo, F. K. Fatemi, K. M. Jones, J. E. Simsarian, D. Cho, A. Simoni, E. Tiesinga, P. S. Julienne, K. Helmerson, P. D. Lett, S. L. Rolston, and W. D. Phillips, *Phys. Rev. Lett.* **88**, 120403 (2002).
- [7] M. Yan, B. J. DeSalvo, Y. Huang, P. Naidon, and T. C. Killian, *Phys. Rev. Lett.* **111**, 150402 (2013).
- [8] M. Junker, D. Dries, C. Welford, J. Hitchcock, Y. P. Chen, and R. G. Hulet, *Phys. Rev. Lett.* **101**, 060406 (2008).
- [9] C.-F. Liu, H. Fan, S.-C. Gou, and W.-M. Liu, *Sci. Rep.* **4**, 4224 (2014).
- [10] Y. J. Lin, K. Jiménez-García, and I. B. Spielman, *Nature (London)* **471**, 83 (2011).
- [11] R. A. Williams, L. J. LeBlanc, K. Jiménez-García, M. C. Beeler, A. R. Perry, W. D. Phillips, and I. B. Spielman, *Science* **335**, 314 (2012).
- [12] S. C. Ji, J.-Y. Zhang, L. Zhang, Z.-D. Du, W. Zheng, Y.-J. Deng, H. Zhai, S. Chen, and J.-W. Pan, *Nat. Phys.* **10**, 314 (2014).
- [13] C. L. Qu, C. Hamner, M. Gong, C. W. Zhang, and P. Engels, *Phys. Rev. A* **88**, 021604(R) (2013).
- [14] C. Hamner, C. L. Qu, Y. P. Zhang, J. J. Chang, M. Gong, C. W. Zhang, and P. Engels, *Nat. Commun.* **5**, 4023 (2014).
- [15] A. J. Olson, S.-J. Wang, R. J. Niffenegger, C.-H. Li, C. H. Greene, and Y. P. Chen, *Phys. Rev. A* **90**, 013616 (2014).
- [16] L. W. Cheuk, A. T. Sommer, Z. Hadzibabic, T. Yefsah, W. S. Bakr, and M. W. Zwierlein, *Phys. Rev. Lett.* **109**, 095302 (2012).
- [17] P. J. Wang, Z.-Q. Yu, Z. K. Fu, J. Miao, L. Huang, S. Chai, H. Zhai, and J. Zhang, *Phys. Rev. Lett.* **109**, 095301 (2012).
- [18] C. Wang, C. Gao, C. M. Jian, and H. Zhai, *Phys. Rev. Lett.* **105**, 160403 (2010).
- [19] T. L. Ho and S. Z. Zhang, *Phys. Rev. Lett.* **107**, 150403 (2011).
- [20] Y. Li, G. I. Martone, L. P. Pitaevskii, and S. Stringari, *Phys. Rev. Lett.* **110**, 235302 (2013).
- [21] S. Gopalakrishnan, I. Martin, and E. A. Demler, *Phys. Rev. Lett.* **111**, 185304 (2013).
- [22] S. Sinha, R. Nath, and L. Santos, *Phys. Rev. Lett.* **107**, 270401 (2011).
- [23] X.-Q. Xu and J. H. Han, *Phys. Rev. Lett.* **107**, 200401 (2011).
- [24] H. Hu, B. Ramachandhran, H. Pu, and X. J. Liu, *Phys. Rev. Lett.* **108**, 010402 (2012).
- [25] X. F. Zhou, J. Zhou, and C. J. Wu, *Phys. Rev. A* **84**, 063624 (2011).
- [26] R. M. Wilson, B. M. Anderson, and C. W. Clark, *Phys. Rev. Lett.* **111**, 185303 (2013).
- [27] V. Achilleos, D. J. Frantzeskakis, P. G. Kevrekidis, and D. E. Pelinovsky, *Phys. Rev. Lett.* **110**, 264101 (2013).
- [28] T. Kawakami, T. Mizushima, M. Nitta, and K. Machida, *Phys. Rev. Lett.* **109**, 015301 (2012).
- [29] V. E. Lobanov, Y. V. Kartashov, and V. V. Konotop, *Phys. Rev. Lett.* **112**, 180403 (2014).

- [30] Y. V. Kartashov, V. V. Konotop, and F. Kh. Abdullaev, *Phys. Rev. Lett.* **111**, 060402 (2013).
- [31] H. Sakaguchi and B. A. Malomed, *Phys. Rev. E* **90**, 062922 (2014).
- [32] C. F. Liu, Y. M. Yu, S. C. Gou, and W. M. Liu, *Phys. Rev. A* **87**, 063630 (2013).
- [33] C. F. Liu, W. J. Wan, and G. Y. Zhang, *Acta Phys. Sin.* **62**, 200306 (2013).
- [34] J. Ruseckas, G. Juzeliūnas, P. Öhberg, and M. Fleischhauer, *Phys. Rev. Lett.* **95**, 010404 (2005).
- [35] T. D. Stanescu and V. Galitski, *Phys. Rev. B* **75**, 125307 (2007).
- [36] G. Juzeliūnas, J. Ruseckas, and J. Dalibard, *Phys. Rev. A* **81**, 053403 (2010).
- [37] B. M. Anderson, G. Juzeliūnas, V. M. Galitski, and I. B. Spielman, *Phys. Rev. Lett.* **108**, 235301 (2012).
- [38] B. M. Anderson, I. B. Spielman, and G. Juzeliūnas, *Phys. Rev. Lett.* **111**, 125301 (2013).
- [39] C. D. Hamley, E. M. Bookjans, G. Behin-Aein, P. Ahmadi, and M. S. Chapman, *Phys. Rev. A* **79**, 023401 (2009).
- [40] J. Kobayashi, Y. Izumi, K. Enomoto, M. Kumakura, and Y. Takahashi, *Appl. Phys. B* **95**, 37 (2009).
- [41] S. J. Rooney, A. S. Bradley, and P. B. Blakie, *Phys. Rev. A* **81**, 023630 (2010).
- [42] A. S. Bradley, C. W. Gardiner, and M. J. Davis, *Phys. Rev. A* **77**, 033616 (2008).
- [43] J. Radic, T. A. Sedrakyan, I. B. Spielman, and V. Galitski, *Phys. Rev. A* **84**, 063604 (2011).
- [44] A. Aftalion and P. Mason, *Phys. Rev. A* **88**, 023610 (2013).
- [45] A. Schmeller, J. P. Eisenstein, L. N. Pfeiffer, and K. W. West, *Phys. Rev. Lett.* **75**, 4290 (1995).
- [46] X. Z. Yu, Y. Onose, N. Kanazawa, J. H. Park, J. H. Han, Y. Matsui, N. Nagaosa, and Y. Tokura, *Nature (London)* **465**, 901 (2010).
- [47] X. Li, W. V. Liu, and L. Balents, *Phys. Rev. Lett.* **112**, 067202 (2014).
- [48] C. F. Liu and W. M. Liu, *Phys. Rev. A* **86**, 033602 (2012).
- [49] C. F. Liu, H. Fan, Y. C. Zhang, D. S. Wang, and W. M. Liu, *Phys. Rev. A* **86**, 053616 (2012).
- [50] K. Kasamatsu, M. Tsubota, and M. Ueda, *Phys. Rev. Lett.* **93**, 250406 (2004).
- [51] S. J. Woo, Q-Han Park, and N. P. Bigelow, *Phys. Rev. Lett.* **100**, 120403 (2008).
- [52] K. Kasamatsu, M. Tsubota, and M. Ueda, *Phys. Rev. A* **71**, 043611 (2005).
- [53] T. Mizushima, K. Machida, and T. Kita, *Phys. Rev. Lett.* **89**, 030401 (2002).
- [54] T. Mizushima, N. Kobayashi, and K. Machida, *Phys. Rev. A* **70**, 043613 (2004).
- [55] See Supplemental Material at <http://link.aps.org/supplemental/10.1103/PhysRevA.95.023624> for the effect of atom-molecule conversion and Raman coupling on the carbon-dioxide-like skyrmion, the approximate solution of the carbon-dioxide-like skyrmion, and the ground state of rotating atomic-molecular BECs without SOC.
- [56] M. Aidelsburger, M. Lohse, C. Schweizer, M. Atala, J. T. Barreiro, S. Nascimbène, N. R. Cooper, I. Bloch, and N. Goldman, *Nat. Phys.* **11**, 162 (2015).
- [57] K. V. Kheruntsyan and P. D. Drummond, *Phys. Rev. A* **58**, R2676 (1998).
- [58] P. D. Drummond, K. V. Kheruntsyan, and H. He, *Phys. Rev. Lett.* **81**, 3055 (1998).
- [59] J. Javanainen and M. Mackie, *Phys. Rev. A* **59**, R3186 (1999).
- [60] S. Inouye, M. R. Andrews, J. Stenger, H.-J. Miesner, D. M. Stamper-Kurn, and W. Ketterle, *Nature (London)* **392**, 151 (1998).
- [61] Ph. Courteille, R. S. Freeland, D. J. Heinzen, F. A. van Abeelen, and B. J. Verhaar, *Phys. Rev. Lett.* **81**, 69 (1998).
- [62] P. D. Drummond, K. V. Kheruntsyan, D. J. Heinzen, and R. H. Wynar, *Phys. Rev. A* **65**, 063619 (2002).
- [63] M. Mackie, R. Kowalski, and J. Javanainen, *Phys. Rev. Lett.* **84**, 3803 (2000).
- [64] E. V. Goldstein, M. G. Moore, H. Pu, and P. Meystre, *Phys. Rev. Lett.* **85**, 5030 (2000).
- [65] A. E. Leanhardt, Y. Shin, D. Kielpinski, D. E. Pritchard, and W. Ketterle, *Phys. Rev. Lett.* **90**, 140403 (2003).
- [66] L. S. Leslie, A. Hansen, K. C. Wright, B. M. Deutsch, and N. P. Bigelow, *Phys. Rev. Lett.* **103**, 250401 (2009).
- [67] J. Y. Choi, W. J. Kwon, and Y. I. Shin, *Phys. Rev. Lett.* **108**, 035301 (2012).
- [68] L. D. Carr, D. DeMille, R. V. Krems, and J. Ye, *New J. Phys.* **11**, 055049 (2009).
- [69] S. Ospelkaus, K.-K. Ni, D. Wang, M. H. G. de Miranda, B. Neyenhuis, G. Quémener, P. S. Julienne, J. L. Bohn, D. S. Jin, and J. Ye, *Science* **327**, 853 (2010).
- [70] T. L. Ho, *Phys. Rev. Lett.* **81**, 742 (1998).
- [71] T. Ohmi and K. Machida, *J. Phys. Soc. Jpn.* **67**, 1822 (1998).